Length of Polarization-Correlation Based on Speckle Pattern for Optical Coherent Detection

Longkun Zhang, Jianfeng Sun, Qian Xu, and Weibiao Chen

***Abstract*—A length of polarization-correlation (LPC) based on speckle pattern of the non-uniform spatial polarization distribution is proposed and measured by using the classical measurement method of the Stokes polarization parameters for optical coherent detection. The LPC, which depends on the material of the scattering medium, is emphasized on the speckle scale. A gradually expanding window centered at the brightest spot of the speckle pattern, is designed to calculate the degree of polarization (DOP) of different speckle sizes. Moreover, the magnitude of LPC is equal to the speckle size that reaches a particular threshold on the DOP curve. It is experimentally demonstrated that the LPC is exploited to not only investigate the nature of the polarization changes between different speckle sizes, but also be combined with coherent efficiency. This study can provide new insights of speckle depolarization in optical coherent detection and open new opportunities for improving coherent efficiency.**

***Index Terms*—Length of polarization-correlation, speckle depolarization, optical coherent detection, coherent efficiency.**

I. Introduction

OPTICAL coherent detection, which takes advantage of the photomixing between local oscillator (LO) and signal lights [1], has been commonly used in the fields of laser communication [2], gravitational waves observation [3], heterodyne spectroscopy [4], and radar systems [5], etc. The focus of the optical coherent detection, such as the intensity and the phase distribution, has been reported to be very useful tool in investigating the spatial coherence property of a scattered light [6], [7], [8]. However, a randomly distributed granular intensity pattern, known as the speckle [9], [10], [11], [12], is generated when the coherent light illuminates on a scattering medium. Furthermore, the polarization state of the backscatter light is spatially scrambled by the multiple scattering media, resulting in the speckle depolarization [13], [14], [15], [16]. The coherent efficiency is a metric for evaluating the performance of the optical coherent detection [17], which not only reflects the matching extent of phase and amplitude between LO and signal lights, but also reveals the polarization matching of two overlapped beams [18], [19]. In other words, the polarization of the scattered light from the rough surface or the diffusive medium is gradually lost [14], which will induce decoherence effect [20] and reduce the coherent efficiency [17], [18], [19].

Although the fact that the local enpolarization of light [21], [22] and the multi-scale depolarization [23], [24] has been emphasized at the speckle size, the polarization characteristic of a speckle is still not paid much attention. And the polarization characteristic of the speckle is found to be carrying the nature of the scattering medium [25], [26]. Besides, the intensity correlation technologies [27], [28], [29] such as the spatial degree of coherence (DOC), the autocorrelation length of the Stokes parameters, and the depolarized speckle pattern (DSP), have also been investigated to characterize the spatial coherence-polarization property of the speckle, but a limited number of efforts are made to combine with coherent efficiency and analyze the speckle depolarization with different speckle sizes. Thus, a new technique needs to be introduced as a bridge between the coherent efficiency and the polarization characteristic of the speckle.

In this article, a length of polarization-correlation (LPC) based on speckle pattern of different scattering media, using the classical measurement method of the Stokes polarization parameters [30], is proposed and measured, which can combine the coherent efficiency with the polarization characteristic of the speckle. The new technique depends on the material of the scattering medium. Furthermore, the LPC is emphasized on the speckle scale, which can investigate the nature of the polarization changes between different speckle sizes. This study can also provide a reference for the design of the coherent efficiency in optical coherent systems. The theoretical analysis and experimental measurement are presented.

II. Experimental Setup and Theoretical Analysis

An incident field at the wavelength of 1.55 μm from the narrow linewidth laser (NLL) is launched into the fiber collimator (FC, Thorlabs: F260APC). After passing through the linear polarizer 1 (P1) and the quarter-wave plate 1 (QWP1), the left circularly polarized light is obtained. Whereafter the light propagates along the liftable quarter-wave plate 2 (QWP2) and the linear polarizer 2 (P2), then is recorded by an 8-bit charge-coupled device (CCD, Xenics: XS-USB-FPA-320) without camera lens, as depicted in Fig. 1(a). The image size of the

Manuscript received 1 January 2024; revised 8 February 2024; accepted 13 February 2024. Date of publication 15 February 2024; date of current version 14 March 2024. *(Corresponding authors: Jianfeng Sun; Weibiao Chen.)*

Longkun Zhang and Weibiao Chen are with the Department of Optics and Optical Engineering, University of Science and Technology of China, Hefei 230026, China, and also with the Key Laboratory of Space Laser Communication and Detection Technology, Shanghai Institute of Optics and Fine Mechanics, Chinese Academy of Sciences, Shanghai 201800, China (e-mail: zhanglongkun@mail.ustc.edu.cn; wbchen@siom.ac.cn).

Jianfeng Sun and Qian Xu are with the Shanghai Key Laboratory of Satellite Network, Shanghai 200120, China (e-mail: sunjianfengs@163.com; xuqian@siom.ac.cn).

Digital Object Identifier 10.1109/JPHOT.2024.3366398

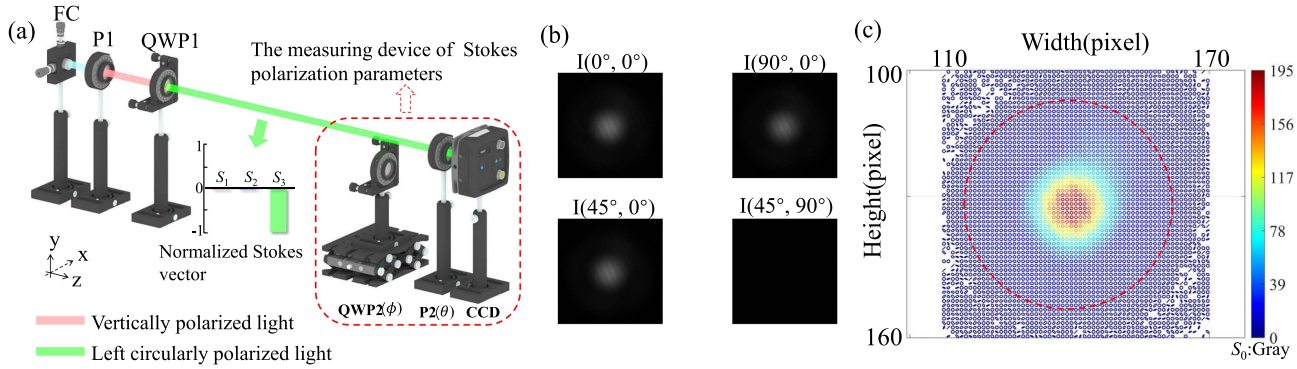

Fig. 1. (a) Setup diagram of Stokes polarimetry. (b) Raw polarization intensity images at four angles by setting θ to 0°, 90° or 45° and ϕ to 0° or 90° with the proper pairings of angles. For example: $I(0°, 0°)$ is the polarization intensity image by setting θ to 0° and ϕ to 0°. (c) Polarization ellipses corresponding to each pixel. FC: fiber collimator, P: linear polarizer, QWP: quarter-wave plate, CCD: charge-coupled device. θ is the rotation angle of the transmission axis of the P2, and ϕ is the phase shift of the QWP2. The image size of (b) and (c) is 61×61 pixels (width pixel range: 110–170; height pixel range: 100–160).

camera is 320×256 pixels (Width $\times$ Height), and the pixel size is $30\,\mu\text{m} \times 30\,\mu\text{m}$.

The red dotted frame in Fig. 1(a) is the measuring device of the Stokes polarization parameters which is sufficient to completely describe the polarization state of the light by analyzing the four Stokes parameters. Furthermore, the first three Stokes parameters (S_0, S_1, S_2) can be obtained by removing the QWP2 $(\phi = 0°)$ and rotating the transmission axis of the P2 to the angles $\theta = 0°$, 90° and 45°, respectively. The final parameter, S_3, is obtained by reinserting the QWP2 ($\phi = 90°$, the fast axis azimuth at 0°) into the optical path and setting the transmission axis of the P2 to $\theta = 45°$. The Stokes parameters corresponding to each pixel are given by [30]:

$$\begin{cases} S_0\ (m,n) = [I\,(0°, 0°)]_{m,n} + [I\,(90°, 0°)]_{m,n} \\ S_1\ (m,n) = [I\,(0°, 0°)]_{m,n} - [I\,(90°, 0°)]_{m,n} \\ S_2\ (m,n) = 2[I\,(45°, 0°)]_{m,n} - S_0\,(m,n) \\ S_3\ (m,n) = 2[I\,(45°, 90°)]_{m,n} - S_0\,(m,n) \end{cases} \tag{1}$$

Here, m and n are the width and height pixel in the CCD image, respectively. $[I(\theta, \phi)]_{m,n}$ represents the gray value of the coordinate point (m, n) in the corresponding polarization intensity images at four angles by setting θ to 0°, 90° or 45° and ϕ to 0° or 90° with the proper pairings of angles.

Fig. 1(b) depicts the raw polarization intensity images at four angles when a left circularly polarized light is generated by rotating the optical axes of the P1 and QWP1. The polarization intensity image of $I(45°, 90°)$ has no light power which agrees well with the theoretical analysis. Besides, the corresponding polarization ellipse is also obtained from the Stokes parameters, which is:

$$\begin{cases} E_x\ (m,n) = \frac{\sqrt{S_1^2(m,n)+S_2^2(m,n)+S_3^2(m,n)}+S_1(m,n)}{2} \\ E_y\ (m,n) = \frac{\sqrt{S_1^2(m,n)+S_2^2(m,n)+S_3^2(m,n)}-S_1(m,n)}{2} \\ \delta\ (m,n) = \delta_y\ (m,n) - \delta_x\ (m,n) = arctan\left[\frac{S_3(m,n)}{S_2(m,n)}\right] \end{cases} \tag{2}$$

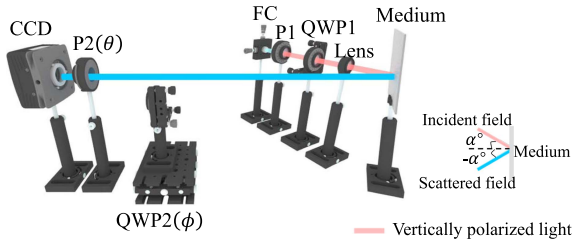

Fig. 2. Setup diagram of the measuring LPC.

$$\begin{cases} \psi\ (m,n) = \frac{1}{2}\ arctan\left[\frac{S_2(m,n)}{S_1(m,n)}\right] \in [0\ ,\pi) \\ \chi\ (m,n) = \frac{1}{2}\ arcsin\left[\frac{S_3(m,n)}{\sqrt{S_1^2(m,n)+S_2^2(m,n)+S_3^2(m,n)}}\right] \\ \quad \in \left[-\frac{\pi}{4}, \frac{\pi}{4}\right] \end{cases} \tag{3}$$

Here, $E_x(m,n)$ and $E_y(m,n)$ are the horizontal and vertical field amplitude of the pixel point (m, n). $\delta(m,n) = \delta_y(m,n) - \delta_x(m,n)$ is the phase difference at the pixel point (m, n). $\delta_y(m,n)$ and $\delta_x(m,n)$ refer to the phase in horizontal and vertical direction, respectively. $\psi(m,n)$ and $\chi(m,n)$ are the orientation angle and the ellipticity angle, separately.

Fig. 1(c) displays the polarization ellipses corresponding to each pixel. And the color of each polarization ellipse is mapped by the corresponding gray value of S_0. The normalized Stokes vectors of each pixel within the red dotted frame in Fig. 1(c) are all $(1, 0, 0, -1)^T$. It means that the polarization states of these ellipses are the left-hand circular polarization. T represents the transpose of the vector. Although the local gray value of S_0 is less than 78 (greater than 6) in the red dotted frame, it is worth noting that the polarization has a weaker dependence with the light intensity. The polarization states of these ellipses outside the red dotted frame (the gray value of S_0 is smaller than 6) are lack of credibility attributing to the low-quality signal-to-noise ratio (SNR). Besides, the linear horizontally, vertically, ±30°, ±45°, ±60° and the right circularly polarized light are also accurately measured by using the measuring device of the Stokes polarization parameters.

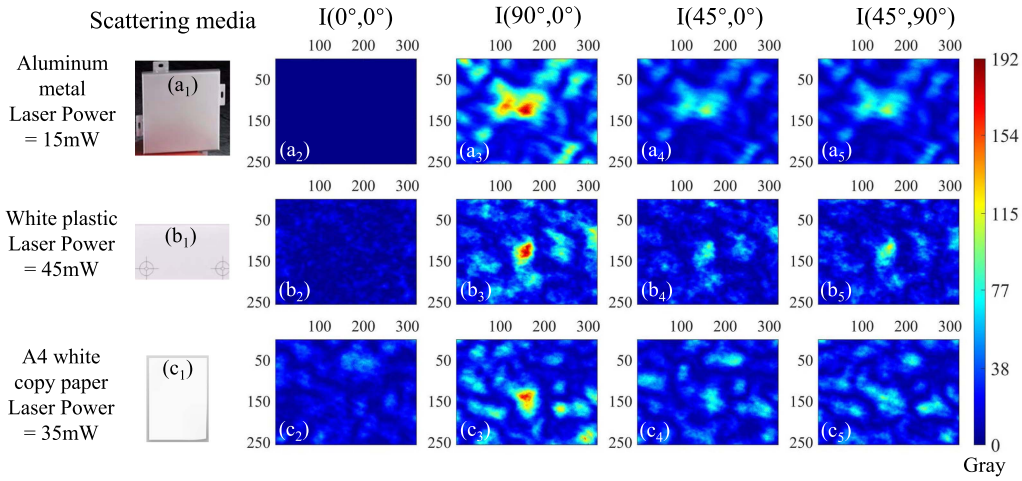

Fig. 3. Schematics of scattering media: aluminium metal (a1), white plastic (b1) and A4 white copy paper (c1). Polarization speckle patterns by setting θ to 0°, 90° or 45° and ϕ to 0° or 90° with the proper pairings of angles for aluminium metal (a2)–(a5), white plastic (b2)–(b5) and A4 white copy paper (c2)–(c5). For example: (a2) is the polarization speckle pattern of $I(0^\circ, 0^\circ)$ by setting θ to 0° and ϕ to 0° using the aluminium metal as the scattering medium. The color bar on the right displays a shared color and maps the gray value to the color images. A sampling time of 30 s is adopted for each polarization speckle patterns.

Fig. 2 shows the schematic diagram of the measuring the LPC based on Stokes polarization parameters. An incident field at the wavelength of 1.55 μm from the NLL is collimated by the FC. After passing through the P1 and QWP1, a completely polarized light is obtained and then focused by a lens (focal length: $f =$ 50 mm). Whereafter the beam illuminates the medium at α° to the normal of medium surface, which is defined as the Z axis. The measuring device of the Stokes polarization parameters, which collects and records the light scattered by the medium, is placed at $-\alpha^\circ$ to the normal of medium surface, simultaneously.

Here, the completely polarized light is emitted as the illuminating beam to generate the polarization speckle patterns. A linear vertically polarized light, commonly utilized and readily accessible, is considered and employed for measuring LPC. Furthermore, there is an inverse proportional relationship between the spot size of the illumination on the scattering medium and the size of the speckle. To improve the measurement accuracy of the speckle patterns, the lens is used to adjust the spot size of the illumination on the scattering medium and generate the large speckle patterns. Because the spot size of the illumination on the scattering media and the average diameter of the speckle are independent of the scattering medium material. Therefore, after obtaining the desired spot size, the lens remains unchanged for different scattering media. It has also been confirmed that the "loss of polarization" is connected with the receiver solid angle [13]. Thus, the $\alpha = 30^\circ$ is designed, which remains unchanged during medium material replacement to have a unified measurement standard in the process of measuring LPC.

The scattering media of different materials are the aluminium metal, the white plastic (the back of the detector card, Thorlabs: VRC2) and the A4 white copy paper (M & G: B640217), as shown in Fig. 3(a1), (b1) and (c1), respectively. The polarization speckle patterns at four angles by setting θ to 0°, 90° or 45° and ϕ to 0° or 90° with the proper pairings of angles for aluminium metal, white plastic and A4 white copy paper are Fig. 3(a2)–(a5), (b2)–(b5) and (c2)–(c5), separately. Considering the different reflectivity of the media, the corresponding power values of the incident field are 15 mW, 45 mW and 35 mW to ensure that the polarization speckle patterns of three media have the same and credible SNR, as displayed in the vertical color bar on the right of Fig. 3.

As expected, the polarization speckle pattern of $I(0^\circ, 0^\circ)$ for aluminium metal has no light power which agrees well with the theoretical analysis using the linear vertically polarized light as the illuminating beam, as shown in Fig. 3(a2). It also means that the metal material is non-depolarization. In Fig. 3(b2) and (c2), the power values of the polarization speckle patterns are non-zero. To put it simply, the white plastic and the A4 white copy paper have the polarization effect which changes the polarization state through the retardance or birefringence effect.

Furthermore, the spot diameter focused and illuminated on the surface of the medium can be expressed as [31]:

$$D = \frac{2}{\cos(30^\circ)} \cdot \sqrt{\frac{\left(1-\frac{l_c}{f}\right)^2\left(\frac{\pi\omega_0^2}{\lambda}\right)^2 + \left(l_c + l - \frac{l l_c}{f}\right)^2}{\left(\frac{\pi\omega_0^2}{\lambda}\right)^2}} = 485.55\,\mu\text{m} \tag{4}$$

Here, $l_c = 57$ mm is the distance between the lens and medium. $\omega_0 = 1.5$ mm and $l = 185$ mm are the waist radius of the incident field and the distance between beam waist and lens, respectively. $\lambda = 1550$ nm refers to the wavelength of the incident field. After passing through the distance $z_1 = 470$ mm, the polarization speckle patterns of the scattered light at four angles by setting θ to 0°, 90° or 45° and ϕ to 0° or 90° with the proper pairings of angles are recorded by the CCD. And the average diameter of the speckle pattern is $d = 2 \cdot 1.22 \cdot \lambda z_1 / D =$ 3.66 mm.

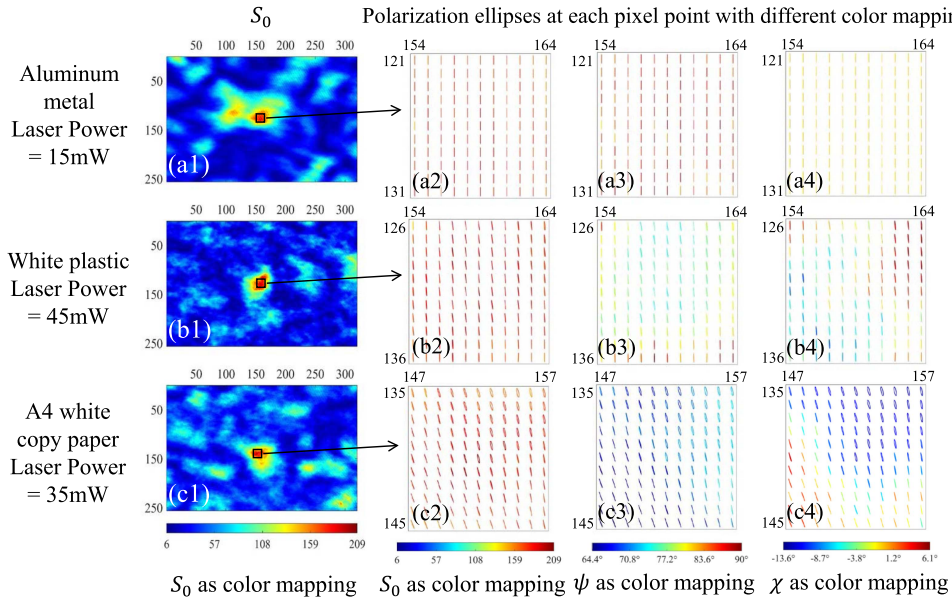

Fig. 4. Full-pixel polarization ellipses of S_0 corresponding to aluminium metal (a1), white plastic (b1) and A4 white copy paper (c1). The locally magnified polarization ellipses of aluminium metal (a2)–(a4), white plastic (b2)–(b4) and A4 white copy paper (c2)–(c4) with different parameters as color mappings, separately. The locally magnified image size is 11×11 pixels near the corresponding S_0 maximum gray.

III. Results and Discussion

Fig. 4(a1), (b1) and (c1), which are calculated by the depicted polarization speckle patterns in Fig. 3, display the full-pixel polarization ellipses of S_0 for the aluminium metal, white plastic and A4 white copy paper, respectively. The color of the full-pixel polarization ellipses is also mapped by the corresponding gray value of S_0. Besides, the pixel coordinates of the S_0 maximum gray based on the media of the metal, the white plastic and A4 white copy paper are $(159, 126)$, $(159, 131)$ and $(152, 140)$, separately. Here, the coordinate format is (Width, Height). Whereafter the locally magnified images of the polarization ellipses with S_0, ψ and χ as color mappings are described in Fig. 4(a2)–(a4), (b2)–(b4) and (c2)–(c4), respectively.

In Fig. 4(a2)–(a4), it is clearly seen that the polarization states of these ellipses ($\psi = 90^\circ$ and $\chi = 0^\circ$) are consistent with the linear vertically polarized illuminating beam, which indicates that the metal material is non-depolarization. The polarization states of these ellipses in Fig. 4(b2)–(b4) and (c2)–(c4) are gradually variable, which means that the white plastic and A4 white copy paper have the polarization effect. Moreover, the variation trend of the polarization ellipses in Fig. 4(c2)–(c4) is more drastic than that in Fig. 4(b2)–(b4).

The Stokes parameters can describe the degree of polarization (DOP) of any polarization state. By definition: $\mathrm{DOP} = \sqrt{S_1^2 + S_2^2 + S_3^2}/S_0 \in [0, 1]$. Concretely, the value of $\mathrm{DOP} = 1$ and $\mathrm{DOP} = 0$ correspond to completely polarized and unpolarized light. $0 < \mathrm{DOP} < 1$ refers to partially polarized light.

When the S_0 gray value is equal to $k (k = 1, 2, 3, \cdots)$, the corresponding DOP can be calculated by:

$$\mathrm{DOP}\left(S_0 = k\right) = \frac{1}{n_k} \sum_{i=1}^{n_k} \left(\mathrm{DOP}\right)_i \tag{5}$$

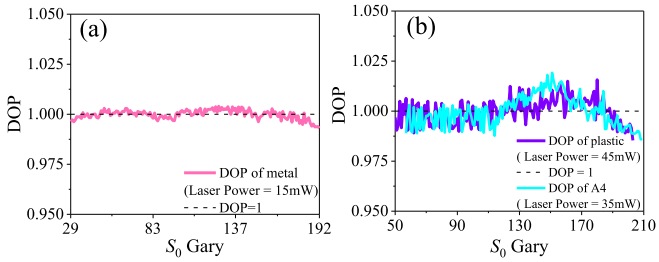

Fig. 5. (a) DOP curve of aluminium metal. And the range of the credible S_0 gray value is not less than 29 attributing to the background noise of CCD for aluminium metal. (b) DOP curves of white plastic and A4 white copy paper. And the ranges of the credible S_0 gray value are not less than 50 and 57 for plastic and A4, separately.

Here, n_k refers to the total number of pixels with $S_0 = k$. $(\mathrm{DOP})_i$ represents the DOP value calculated by the ith pixel of $S_0 = k$. Moreover, the optimal amount of the speckle patterns information required for achieving high measurement accuracy can be determined by the SNR of the speckle patterns. And the SNR is directly proportional to $\frac{N_s}{N_n}$. Here, N_s refers to the number of pixels where DOP converges to 1 ($0.98 \leq \mathrm{DOP} \leq 1.02$). N_n is the number of pixels exclusive of N_s.

The DOP curve is shown in Fig. 5(a) using the aluminium metal as the scattering medium when the power value of the incident field is 15 mW. The minimum measurable polarization information of the speckle pattern is limited by the background noise of CCD. And the DOP curve of the aluminium metal converges to $\mathrm{DOP} = 1$ in the credible range of S_0 gray value (29-192). Similarly, Fig. 5(b) shows the DOP curves using the white plastic and A4 white copy paper as the scattering media when the power values of the incident field are 45 mW and 35 mW, respectively. The ranges of the credible gray value

are considered to be not less than 50 and 57 for the white plastic and A4 white copy paper, separately. It is worth noting that the exposure times of CCD are 100 μs, 500 μs and 600 μs for aluminium metal, white plastic and A4 white copy paper, respectively. When the exposure time is 100 μs, the statistical results of 1000 times indicate that the background noise follows a normal distribution with a mean of 20 and a variance of 2.28. And the background noise of CCD also increases with the extension of the exposure time. Hence, the credible gray ranges of the white plastic and A4 white copy paper are smaller than that of the aluminium metal.

After obtaining the pixel coordinate of the S_0 maximum gray and the range of the credible gray value, the LPC is calculated and emphasized on the speckle scale. And the magnitude of LPC is equal to the speckle size that reaches 0.9 on the DOP curve. A square window, which has a central coordinate (W_0, H_0) placed in the coordinate point of the S_0 maximum gray, is extended within the range of the credible gray value. Furthermore, to ensure that each pixel has the same physical contribution in the window, the method of the polarization component intensity normalization is designed.

For example, the size of window is assumed to be $a \times a$ pixels ($a = 1, 3, 5, \ldots, 255$), and the gray values of each pixel in the window are all confined in the range of the credible gray value. Thus, the normalized polarization component intensity of each pixel can be expressed as:

$$[I'(\theta,\phi)]_{m,n} = \frac{[I(\theta,\phi)]_{m,n}}{[I(0^\circ,0^\circ)]_{m,n} + [I(90^\circ,0^\circ)]_{m,n}} \tag{6}$$

Here, $[I'(\theta,\phi)]_{m,n}$ is the normalized polarization component intensity of the coordinate point (m, n) in the corresponding polarization speckle patterns at four angles by setting θ to 0°, 90° or 45° and ϕ to 0° or 90° with the proper pairings of angles. $[I(0^\circ,0^\circ)]_{m,n} + [I(90^\circ,0^\circ)]_{m,n}$ is the total intensity of the coordinate point (m, n).

Then, the Stokes parameters in the window can be expressed as: (7) shown at the bottom of the page.

The DOP in the window ($a \times a$ pixels) is given by:

$$\mathrm{DOP} = \frac{\sqrt{S_1'^2 + S_2'^2 + S_3'^2}}{S_0'} \tag{8}$$

Fig. 6(a) is the three-dimensional surface of S_0 using the metal material when the power values of the incident field is 15 mW. The coordinate of the highest point is $(159, 126, 192)$, which agrees well with the coordinate point of the S_0 maximum gray in the Fig. 4(a1). The profile curve of S_0 is obtained by keeping the height at 126 pixels, as depicted in Fig. 6(b). Moreover, the black dotted line, which represents the minimum credible gray value of metal material, has two intersections with the profile curve of S_0 (blue curve). It indicates that the size of the window extending from the central coordinate is limited by the $2{\cdot}min\{(159-43),(248-159)\}+1$. Simply, the maximum size of the extended window is $a_{max} = 2 \times (248 - 159) + 1 = 179$ pixels for metal material.

Subsequently, the curve of the DOP is calculated by averaging the DOP values of the same window size with different powers, as shown in Fig. 6(c1). Although the $a_{max} = 179$ pixel is considered in Fig. 6(c1), the metal material is non-depolarization. As expected, the average DOP curve of metal has no dependence with the size of window. Besides, the polarization states of different window sizes are consistent with the linear vertically polarized illuminating beam, as illustrated in the inset of Fig. 6(c1). It means that the LPC of the metal material is much larger than its own speckle scale.

Similarly, the curves between the DOP and window size using the white plastic and A4 white copy paper as the scattering media are described in Fig. 6(c2) and (c3), respectively. And the maximum size of the extended window is 77 pixel and 65 pixels for the white plastic and A4 white copy paper, separately. As the window size increases, the DOP curves gradually drop in Fig. 6(c2) and (c3), which indicates that the scattered light in the window gradually becomes the partially polarized light. It also means that the white plastic and A4 white copy paper are depolarization. Furthermore, the downward trend of the DOP curve in Fig. 6(c3) is more drastic than that in Fig. 6(c2). In other words, the degree of depolarization using the A4 white copy paper as a scattering medium is more evident than that of white plastic in the same case. The insets of the black curve in Fig. 6(c2) and (c3) are the polarization ellipse of the coordinate point (W_0, H_0). The insets of the pink curve represent the polarization ellipse of the DOP = 0.9. And the polarization ellipses of the pixel coordinate (W_0, H_0) and the DOP = 0.9 exhibit nearly identical polarization states. Therefore, the LPC of the white plastic and A4 white copy paper are 55 pixels ($55 \times 30\,\mu$m = 1.65 mm) and 47 pixels ($47 \times 30\,\mu$m = 1.41 mm), separately.

The coherent efficiency is referred as a measure of the quality in assessing the mixing efficiency of the two overlapped

$$\begin{cases} S_0' = \frac{1}{a^2} \sum\limits_{m=W_0-\frac{a-1}{2}}^{W_0+\frac{a-1}{2}} \sum\limits_{n=H_0+\frac{a-1}{2}}^{H_0+\frac{a-1}{2}} [I'(0^\circ,0^\circ)]_{m,n} + \frac{1}{a^2} \sum\limits_{m=W_0-\frac{a-1}{2}}^{W_0+\frac{a-1}{2}} \sum\limits_{n=H_0+\frac{a-1}{2}}^{H_0+\frac{a-1}{2}} [I'(90^\circ,0^\circ)]_{m,n} \\ S_1' = \frac{1}{a^2} \sum\limits_{m=W_0-\frac{a-1}{2}}^{W_0+\frac{a-1}{2}} \sum\limits_{n=H_0+\frac{a-1}{2}}^{H_0+\frac{a-1}{2}} [I'(0^\circ,0^\circ)]_{m,n} - \frac{1}{a^2} \sum\limits_{m=W_0-\frac{a-1}{2}}^{W_0+\frac{a-1}{2}} \sum\limits_{n=H_0+\frac{a-1}{2}}^{H_0+\frac{a-1}{2}} [I'(90^\circ,0^\circ)]_{m,n} \\ S_2' = \frac{2}{a^2} \sum\limits_{m=W_0-\frac{a-1}{2}}^{W_0+\frac{a-1}{2}} \sum\limits_{n=H_0+\frac{a-1}{2}}^{H_0+\frac{a-1}{2}} [I'(45^\circ,0^\circ)]_{m,n} - S_0' \\ S_3' = \frac{2}{a^2} \sum\limits_{m=W_0-\frac{a-1}{2}}^{W_0+\frac{a-1}{2}} \sum\limits_{n=H_0+\frac{a-1}{2}}^{H_0+\frac{a-1}{2}} [I'(45^\circ,90^\circ)]_{m,n} - S_0' \end{cases} \tag{7}$$

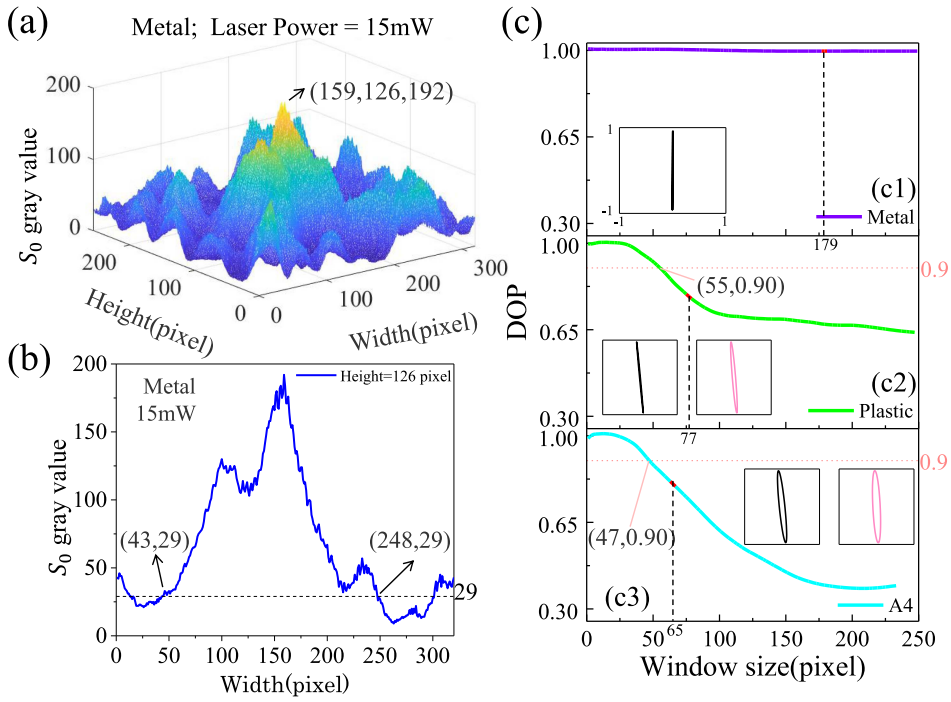

Fig. 6. (a) Three-dimensional surface of S_0. (b) The profile curve of S_0 (Height = 126 pixels) limiting window size. (c1)–(c3) The curves of the DOP and window size using the different media. The insets show the polarization ellipses of the pixel coordinate (W_0, H_0) (black) and the DOP = 0.9 (pink), respectively.

beams on the detector surface [17], [18], [19]. And the coherent efficiency is also associated with the polarization state except the beam's parameters [18]. Assuming the interference is obtained between the scattered light field and the LO beam with linear vertical polarization. To establish the relations between the coherent efficiency and the polarization states, the $\eta_{lpc} = |E_S'|/|E_S| \in [0, 1]$ is defined as the polarization coefficient of the coherent efficiency. Here, E_S' refers to the polarized projection component of the scattered light field to the LO beam. E_S is the normalized complex field function of the scattered light field. The coherent efficiency can be written as:

$$\eta = \eta_{lpc} \cdot \frac{\{\iint |E_s||E_L|\cos\varphi dA\}^2 + \{\iint |E_s||E_L|\sin\varphi dA\}^2}{\iint |E_S|^2 dA \cdot \iint |E_L|^2 dA} \quad (9)$$

Here, E_L represents the normalized complex field function of the LO beam. φ refers to the phase difference between the scattered light field and the LO beam. A is the photosensitive area of the detector.

The scattered light field and the LO beam have almost the same polarization state within the LPC. Hence, the $\eta_{lpc} \approx 1$ when the size of the scattered light field is limited within the LPC. The polarization correlation is also maximum within LPC. After the size of the scattered light field exceeds the LPC, the polarized projection component of the scattered light field to the LO beam gradually decreases, which will induce decoherence effect and reduce the coherent efficiency. The polarization correlation also gradually decreased. Furthermore, the coherent efficiency and polarization changes in free space have been integrally discussed [17], [18].

IV. Conclusion

In summary, we proposed and demonstrated a potential technique using the classical measurement method of the Stokes polarization parameters, referred to as the LPC, which is expected to be a bridge between the coherent efficiency and the polarization characteristic of the speckle. A gradually expanding window is designed to calculate the degree of polarization (DOP) of different speckle sizes. And the magnitude of LPC is defined as the speckle size that reaches 0.9 on the DOP curve. The nature of the polarization change between different speckle sizes can be investigated by using the LPC parameter. Within the LPC, the scattered light field and the LO beam exhibit nearly identical polarization states. After the size of the scattered light field exceeds the LPC, the polarized projection component of the scattered light field to the LO beam gradually decreases, resulting in the decoherence effect. Moreover, the polarization component intensity normalization is also used to ensure that each pixel has the same physical contribution in the process of calculating the LPC. It is observed that the LPC of the metal is much larger than its own speckle scale due to the non-depolarization of metal material. The LPC of the white plastic and the A4 white copy paper is 55 pixels (1.65 mm) and 47 pixels (1.41 mm), respectively.

The LPC can set a foundation for further work in understanding the mechanism of speckle depolarization and improve coherent efficiency for optical coherent detection. Concretely, it can provide a reference for the design of coherent efficiency in optical coherent system. The echo receiving aperture of coherent

system and the polarization state of the LO beam can be designed based on the LPC of different materials, which will improve the coherent efficiency.

REFERENCES

[1] T. Pfeifer, L. Gallmann, M. J. Abel, P. M. Nagel, D. M. Neumark, and S. R. Leone, "Heterodyne mixing of laser fields for temporal gating of high-order harmonic generation," *Phys. Rev. Lett.*, vol. 97, no. 16, Oct. 2006, Art. no. 163901, doi: 10.1103/PhysRevLett.97.163901.

[2] K. Kikuchi, "Fundamentals of coherent optical fiber communications," *J. Lightw. Technol.*, vol. 34, no. 1, pp. 157–179, Jan. 2016, doi: 10.1109/JLT.2015.2463719.

[3] B. P. Abbott et al., "Observation of gravitational waves from a binary black hole merger," *Phys. Rev. Lett.*, vol. 116, no. 6, Feb. 2016, Art. no. 061102, doi: 10.1103/PhysRevLett.116.061102.

[4] Y. Ren et al., "High-resolution heterodyne spectroscopy using a tunable quantum cascade laser around 3.5 THz," *Appl. Phys. Lett.*, vol. 98, no. 23, Jun. 2011, Art. no. 231109, doi: 10.1063/1.3599518.

[5] Q. Guo, K. Yin, T. Chai, X. Ying, and C. Ji, "Photonics-based broadband radar with coherent receiving for high-resolution detection," *IEEE Photon. Technol. Lett.*, vol. 35, no. 14, pp. 745–748, Jul. 2023, doi: 10.1109/LPT.2023.3275958.

[6] G. Maisano, F. Mallamace, P. Migliardo, and F. Wanderlingh, "Linewidth and coherence properties of scattered light," *Opt. Commun.*, vol. 13, no. 4, pp. 405–408, Apr. 1975, doi: 10.1016/0030-4018(75)90133-9.

[7] V. Turzhitsky, J. D. Rogers, N. N. Mutyal, H. K. Roy, and V. Backman, "Characterization of light transport in scattering media at subdiffusion length scales with low-coherence enhanced backscattering," *IEEE J. Sel. Topics Quantum Electron.*, vol. 16, no. 3, pp. 619–626, May/Jun. 2010, doi: 10.1109/JSTQE.2009.2032666.

[8] X. Sun et al., "A criterion for imaging correlography based on optical properties of dynamic multiple scattering media," *Opt. Commun.*, vol. 490, Jul. 2021, Art. no. 126894, doi: 10.1016/j.optcom.2021.126894.

[9] H. Chang, W. Huang, F. Yang, H. Ming, and J. Xie, "Speckle analysis in laser scanning display system," *Chin. Opt. Lett.*, vol. 7, no. 9, pp. 764–767, Sep. 2009, doi: 10.3788/COL20090709.0764.

[10] A. Roy, R. K. Singh, and M. M. Brundavanam, "Controlled modulation of depolarization in laser speckle," *Opt. Lett.*, vol. 42, no. 21, pp. 4343–4346, Nov. 2017, doi: 10.1364/OL.42.004343.

[11] Y. Liu et al., "Modeling the heterodyne efficiency of array detector systems in the presence of target speckle," *IEEE Photon. J.*, vol. 11, no. 4, Aug. 2019, Art. no. 4801509, doi: 10.1109/JPHOT.2019.2925846.

[12] Z. Tang, F. Wang, Z. Fu, S. Zheng, Y. Jin, and G. Situ, "DeepSCI: Scalable speckle correlation imaging using physics-enhanced deep learning," *Opt. Lett.*, vol. 48, no. 9, pp. 2285–2288, May 2023, doi: 10.1364/OL.484867.

[13] C. Amra, M. Zerrad, L. Siozade, G. Georges, and C. Deumié, "Partial polarization of light induced by random defects at surfaces or bulks," *Opt. Exp.*, vol. 16, no. 14, pp. 10372–10354, Jul. 2008, doi: 10.1364/OE.16.010372.

[14] M. Zerrad, J. Sorrentini, G. Soriano, and C. Amra, "Gradual loss of polarization in light scattered from rough surfaces: Electromagnetic prediction," *Opt. Exp.*, vol. 18, no. 15, pp. 15832–15843, Jul. 2010, doi: 10.1364/OE.18.015832.

[15] X. Zhou, G. Gu, K. Ren, W. Qian, J. Xu, and J. Zhang, "Scattering mechanism-based decomposition model for depolarization," *Opt. Commun.*, vol. 458, Mar. 2020, Art. no. 124832, doi: 10.1016/j.optcom.2019.124832.

[16] A. Roy and M. M. Brundavanam, "Polarization-based intensity correlation of a depolarized speckle pattern," *Opt. Lett.*, vol. 46, no. 19, pp. 4896–4899, Oct. 2021, doi: 10.1364/OL.438372.

[17] M. Salem and J. P. Rolland, "Effects of coherence and polarization changes on the heterodyne detection of stochastic beams propagating in free space," *Opt. Commun.*, vol. 281, no. 20, pp. 5083–5091, Oct. 2008, doi: 10.1016/j.optcom.2008.07.015.

[18] Y. Yang, C. Yan, C. Hu, and C. Wu, "Modified heterodyne efficiency for coherent laser communication in the presence of polarization aberrations," *Opt. Exp.*, vol. 25, no. 7, pp. 7567–7591, Apr. 2017, doi: 10.1364/OE.25.007567.

[19] D. Nopchinda, T. Xu, R. Maher, B. C. Thomsen, and I. Darwazeh, "Dual polarization coherent optical spectrally efficient frequency division multiplexing," *IEEE Photon. Technol. Lett.*, vol. 28, no. 1, pp. 83–86, Jan. 2016, doi: 10.1109/LPT.2015.2485669.

[20] X. Dong, Y. Hu, and S. Xu, "Analysis of coherent laser echo characteristics back scattered from rough Gaussian target," *Optik*, vol. 253, Mar. 2022, Art. no. 168512, doi: 10.1016/j.ijleo.2021.168512.

[21] J. Sorrentini, M. Zerrad, G. Soriano, and C. Amra, "Enpolarization of light by scattering media," *Opt. Exp.*, vol. 19, no. 22, pp. 21313–21320, Oct. 2011, doi: 10.1364/OE.19.021313.

[22] G. Soriano, M. Zerrad, and C. Amra, "Enpolarization and depolarization of light scattered from chromatic complex media," *Opt. Exp.*, vol. 22, no. 10, pp. 12603–12613, May 2014, doi: 10.1364/OE.22.012603.

[23] J. Li, G. Yao, and L. V. Wang, "Degree of polarization in laser speckles from turbid media: Implications in tissue optics," *J. Biomed. Opt.*, vol. 7, no. 3, pp. 307–312, Jul. 2002, doi: 10.1117/1.1483313.

[24] J. Broky and A. Dogariu, "Correlations of polarization in random electromagnetic fields," *Opt. Exp.*, vol. 19, no. 17, pp. 15711–15719, Aug. 2011, doi: 10.1364/OE.19.015711.

[25] S. Y. Lu and R. A. Chipman, "Interpretation of Mueller matrices based on polar decomposition," *J. Opt. Soc. Amer. A*, vol. 13, no. 5, pp. 1106–1113, May 1996, doi: 10.1364/JOSAA.13.001106.

[26] Y. Dong et al., "Deriving polarimetry feature parameters to characterize microstructural features in histological sections of breast tissues," *IEEE Trans. Biomed. Eng.*, vol. 68, no. 3, pp. 881–892, Mar. 2021, doi: 10.1109/TBME.2020.3019755.

[27] G. Basso, L. Oliveira, and I. Vidal, "Complete characterization of partially coherent and partially polarized optical fields," *Opt. Lett.*, vol. 39, no. 5, pp. 1220–1222, Mar. 2014, doi: 10.1364/OL.39.001220.

[28] O. Korotkova and E. Wolf, "Generalized stokes parameters of random electromagnetic beams," *Opt. Lett.*, vol. 30, no. 2, pp. 198–200, Jan. 2005, doi: 10.1364/OL.30.000198.

[29] G. R. Salla, V. Kumar, Y. Miyamoto, and R. Singh, "Scattering of Poincaré beams: Polarization speckles," *Opt. Exp.*, vol. 25, no. 17, pp. 19886–19893, Aug. 2017, doi: 10.1364/OE.25.019886.

[30] B. Schaefer, E. Collett, R. Smyth, D. Barrett, and B. Fraher, "Measuring the Stokes polarization parameters," *Amer. J. Phys.*, vol. 75, no. 2, pp. 163–168, Feb. 2007, doi: 10.1119/1.2386162.

[31] S. A. Self, "Focusing of spherical Gaussian beams," *Appl. Opt.*, vol. 22, no. 5, pp. 658–661, Mar. 1983, doi: 10.1364/AO.22.000658.